Instrumentation Mesure Métrologie
Vol. 23, No. 5, October, 2024, pp. 375-382
Journal homepage: http://iieta.org/journals/i2m

Transient Analysis of a Flat-Plate Direct Absorption Solar Collector with Nanofluids

Bernardo Buonomo[1], Leonor Hernández López[2], Oronzio Manca[1*], Gianluca Sarli[1]

[1] Dipartimento di Ingegneria, Università degli studi della Campania "Luigi Vanvitelli", Aversa 81031, Italy
[2] Departamento Ingeniería Mecánica y Construcción, Universitat Jaume I, Castellón de la Plana 12071, Spain

Corresponding Author Email: oronzio.manca@unicampania.it

https://doi.org/10.18280/i2m.230505

Received: 6 July 2024
Revised: 11 September 2024
Accepted: 2 October 2024
Available online: 25 October 2024

Keywords:
nanofluids, solar collectors, direct absorption, carbon nanohorns, transient analysis

ABSTRACT

The thermal performance of a direct absorption solar collector (DASC) can be improved by enhancing the absorbing plate or the effectiveness of the heat transfer fluid. This can be achieved by using a nanofluid instead of pure water, as it possesses better optical properties. This paper conducts numerical simulations on a two-dimensional transient forced convection inside a DASC with a horizontal channel to predict its transient thermal behavior in a specific geographical location under varying hourly solar radiation. The working fluid used is a nanofluid comprised of water and carbon nanohorn nanoparticles, with concentrations ranging from 0 (pure water) to 0.05 g/L. Additionally, the inlet mass flow rate has five varying values from 0.001 to 0.2 kg/s. Results detailing temperature and system efficiency are presented, with their evolution throughout the day also reported. The analysis indicates that the system's performance improves with increasing concentration for each inlet mass flow rate value. Conversely, keeping the concentration constant, the temperature rises as the inlet mass flow rate decreases.

1. INTRODUCTION

Flat-plate solar collectors are a promising solution to meet the thermal energy requirements of both industrial and domestic sectors [1]. Their thermal performance can be improved by enhancing the absorbing plate or the effectiveness of the heat transfer fluid. However, limited contact area between the fluid and solid surface and the low thermal conductivity of common fluids such as water create restrictions in their application, particularly in specialized thermal devices like flat panel solar collectors. To overcome these limitations, direct or volumetric absorption solar collectors (DASC) have been suggested to improve heat exchanges within conventional solar collectors, using a semi-transparent fluid that acts as both an absorber and heat transfer medium [2].

On the other hand, a more effective working fluid, such as a nanofluid, can be utilized. Research on these fluids containing nanoparticles began approximately thirty years ago, with the study conducted by Masuda et al. [3]. Then, the term “nanofluid” was first used by Choi and Eastman [4]. Furthermore, the advancement of nanotechnology has facilitated the reduction of particle size with dimension under 100 nm, allowing for improved suspension stability and increased heat exchange efficiency due to greater nanoparticle surface area. Hence, nanofluid research has become increasingly important in improving the thermal performance of flat-plate solar collectors.

In 2009, Otanicar et al. [5] proposed the term “solar nanofluids” for fluids containing nanoparticles that can enhance optical properties. Various materials have been utilized as nanoparticles for solar nanofluids, including gold [6, 7], paraffin [8], and even red mud [9]. Additionally, alternative base fluid to water, like ethylene glycol [10], have also been investigated.

One of the most promising types of solar nanofluids is Single Wall Carbon Nano Horns (SWCNH). The utilization of nanocarbons has a wide range of applications. A comprehensive review of potential applications in solar thermal energy is provided by Çobanoğlu et al. [11], which covers solar collectors, photovoltaic systems, and solar stills. Recently, their application in batteries has also been explored [12]. Several investigations have been conducted to assess and address the various challenges associated with the use of CNT in DASC [13-16].

However, the majority of the most recent works proposed an experimental approach [17-20], yielding limited results in terms of inlet flow rate and concentration of the nanoparticles, or have investigated other kinds of collectors, like the triple-wall evacuated tube [21], or conducted a steady-state analysis [22].

A comprehensive analysis of the state-of-the-art in solar collectors with nanofluids was recently presented by Hasan et al. [23]. They identified certain gaps in understanding this relatively new system, such as the influence of varying parameters like the aspect ratio of the collector or the characteristics of the nanofluid employed.

This paper conducts numerical simulations on the transient thermal behavior of a flat direct-absorbing solar collector utilizing SWCNH as the working fluid and taking into account the collector's location in a specific geographical area for hourly solar radiation data.

2. PROBLEM DESCRIPTION

2.1 Geometry

A two-dimensional (2D) geometry of the direct absorption flat-plate solar collector is considered with SWCNH-water nanofluid as the working fluid. As depicted in Figure 1, this system consists of two parallel plates with a distance *H* of 0.0012 m and a length *L* of 1 m. The channel runs parallel to the horizontal plane. The top of the collector is covered with glass, considered semi-transparent with a transmissivity ε=0.95, while the bottom plate, made of steel, is considered be adiabatic with the characteristic of a reflector, having an internal emissivity of 0.1. Solar irradiation impinges orthogonally on the surface of the glass plate and diffuses from top to bottom through the volume of the nanofluid. The free stream temperature and the external radiation temperature are set to 288.15 K and 270.15 K, respectively, while the external heat transfer coefficient *h* is 10 W m^{-2} K^{-1}.

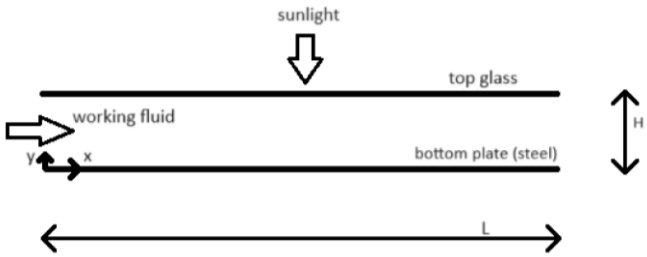

Figure 1. Domain of the system

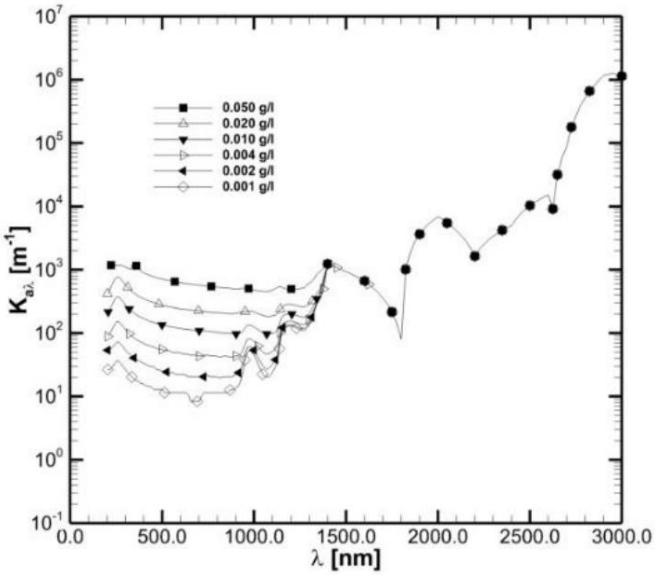

Figure 2. Extinction coefficients of the nanofluids

Seven values of concentration of the carbon nanohorns in base fluid are considered, ranging from 0 (pure water) to 0.05 g L^{-1}. On the other hand, five different values of inlet mass flow rate (MFR) are considered, ranging from 0.001 to 0.2 m^3 s^{-1}. Extinction coefficients K as function of the wavelength and the concentration are given by Sani et al. [24] and presented in Figure 2. The refractive index n of the nanofluid is a function of the wavelength as well, but the values of concentration considered the difference with pure water is negligible [25]. Values by Hale and Querry [26] for the water have then been used for the refractive index of the nanofluid and shown in Figure 3.

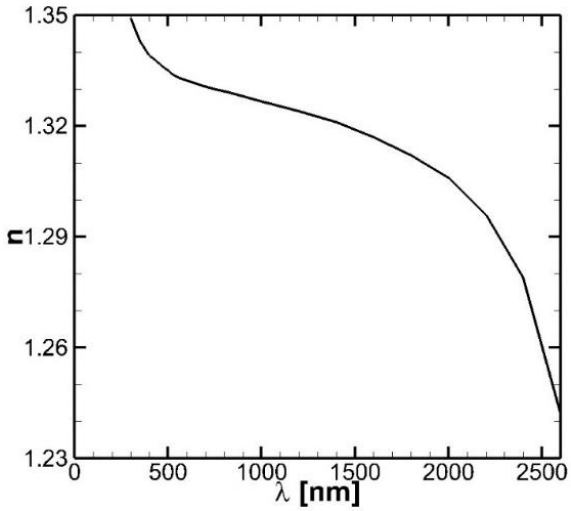

Figure 3. Refractive index

2.2 Governing equations

The forced flow inside the collector is assumed to be transient, laminar, and incompressible. All thermophysical properties are temperature independent and the viscous dissipation is neglected. Gravity is neglected as well since the collector has a horizontal section. Under these hypotheses, the governing equations can be written. They are the continuity Eq. (1), the momentum equation along x and y (2-3) and the energy Eq. (4).

$$\frac{\partial u}{\partial x}+\frac{\partial v}{\partial y}=0 \tag{1}$$

$$\frac{\partial u}{\partial t}+u\frac{\partial u}{\partial x}+v\frac{\partial u}{\partial y}=-\frac{1}{d_{nf}}\frac{\partial p}{\partial x}+\nu_{nf}\left(\frac{\partial^2 u}{\partial x^2}+\frac{\partial^2 u}{\partial y^2}\right) \tag{2}$$

$$\frac{\partial v}{\partial t}+u\frac{\partial v}{\partial x}+v\frac{\partial v}{\partial y}=-\frac{1}{d_{nf}}\frac{\partial p}{\partial y}+\nu_{nf}\left(\frac{\partial^2 v}{\partial x^2}+\frac{\partial^2 v}{\partial y^2}\right) \tag{3}$$

$$\frac{\partial T}{\partial t}+u\frac{\partial T}{\partial x}+v\frac{\partial T}{\partial y}=\frac{k_{nf}}{d_{nf}c_{p,nf}}\left(\frac{\partial^2 T}{\partial x^2}+\frac{\partial^2 T}{\partial y^2}\right)-\frac{1}{d_{nf}c_{p,nf}}\frac{\partial q_R}{\partial y} \tag{4}$$

The coefficients of the governing equations are the thermophysical properties of the nanofluid. However, due to the low concentration of nanoparticles, properties of the base fluid (water) can be used. They are reported in Table 1, along with the properties of the transparent top glass and the bottom plate.

Table 1. Properties of the materials used

	Nanofluid	Glass	Steel
d (kg m^{-3})	998.2	2,200	8,030
c_p (J kg^{-1} K^{-1})	4,182	830	502.48
k (W m^{-1} K^{-1})	0.6	1.2	16.27
μ (Pa s)	$1.003*10^{-3}$	-	-
N	f(λ)	1.471	1

The radiative term of the equation of energy is considered only in the y direction since the radiation is assumed to be one-dimensional, in the direction perpendicular to collector. The radiative heat flux q_R can be calculated as:

$$q_R = 2\pi \int I_\lambda d\lambda \tag{5}$$

The term I_λ is defined by the radiative transfer equation (RTE):

$$\frac{dI_\lambda}{dy} = -K_{a,\lambda}^{nf} I_\lambda(y) + K_{e,\lambda}^{nf} I_{b,\lambda}(T,y) + \frac{K_{s,\lambda}^{nf}}{4\pi} \int_0^{4\pi} I_\lambda(y,\omega_i) f_\lambda(\omega,\omega_i) d\omega_i \tag{6}$$

However, neglecting emission and scattering terms, and taking into account only the decay in the radiation intensity, the RTE becomes the simpler Beer-Lambert law:

$$\frac{I_\lambda}{I_0} = e^{-Ky} \tag{7}$$

In order to solve the governing equation, boundary conditions are needed. They are presented in Table 2.

Table 2. Boundary conditions

Inlet	Bottom Wall	Exit	Top Wall
$u = u_i$	$u = v = 0$	$p = p_{atm}$	$u = v = 0$
$v = 0$	$\frac{\partial T}{\partial y} = 0$		$-k_{nf} \frac{\partial T}{\partial y} = h\Delta T$
$T = 288.15K$ $I_\lambda(y^+) = \rho_b I_\lambda(y^-)$			$I_\lambda(y^-) = \tau_g I_{sol,\lambda} + \rho_g I_\lambda(y^+)$

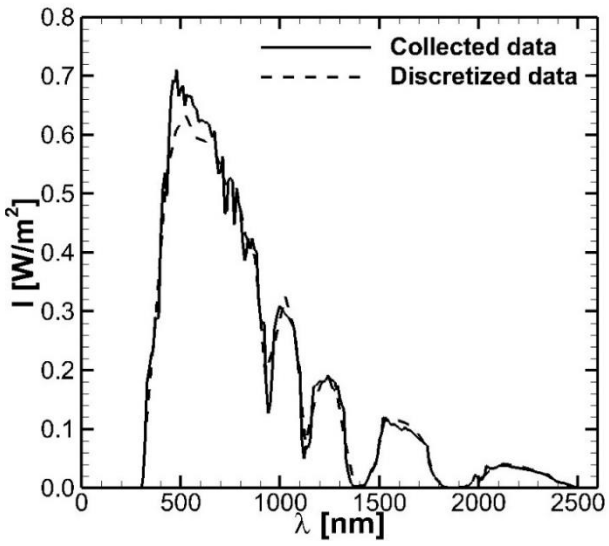

Figure 4. Radiation spectrum (h 12:00)

2.3 Radiation data

Data from Aversa, Italy (40.969 N, 14.208 E) on June 21, 2020, have been collected using the solar spectrum calculator PV Lighthouse [27] for every hour and for a range of wavelengths from 300 to 4,000 nm, with an interval of 10 nm for every band. This spectrum has been then discretized in 46 bands of 25 nm, ranging from 300 to 2,600 nm (the values of the emission outside this range has been considered negligible) in order to implement the Discrete Ordinates (DO) model into the code. An example with the radiation at noon is reported in Figure 4.

2.4 Numerical model

The governing equations were numerically solved using the finite volume method with the ANSYS Fluent (2020 R2 version) [28] commercial code in 2D mode, employing the "Double Precision" option. The Semi Implicit Method for Pressure-Linked Equation (SIMPLE) [29] was used to couple pressure and velocity components in a laminar and incompressible flow.

A mesh made up of 80,000 rectangular cells (4,000 horizontal divisions and 20 vertical divisions) has been implemented.

For the radiative heat transfer the DO model has been implemented. It includes effects of absorbing, emission and scattering of a 2D geometry. As stated above, solar spectrum has been discretized in 46 bands of 50 nm each, ranging from 300 to 2,600 nm and average values of light intensity, refractive index, and extinction coefficient have been implemented into the code.

A second-order upwind scheme was utilized to treat the convective terms in both momentum and energy Eqs. (2)-(4), while a second order central difference scheme was employed for discretization of diffusive terms. For the DO intensity a first order upwind scheme was used instead. The transient formulation has been set as first order implicit. The residuals to satisfy the assigned converging criteria are chosen as 10^{-5} for continuity and velocity components, 10^{-8} for energy, and 10^{-6} for the RTE.

The duration of the daytime, 52,400 seconds, has been divided into 524 time steps of 100 seconds each.

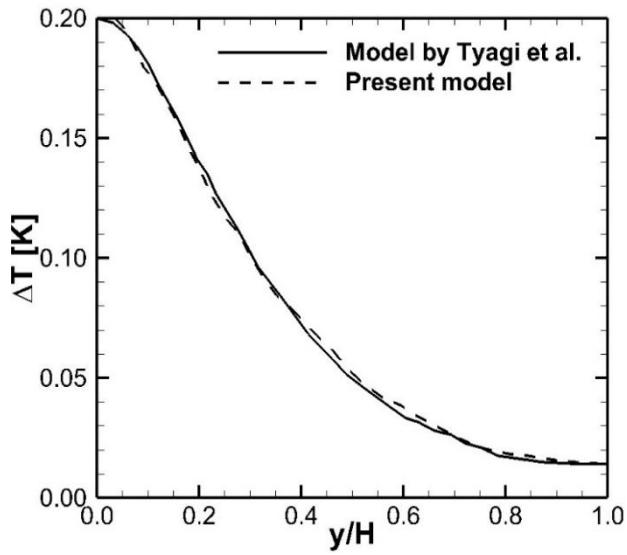

Figure 5. Temperature profile at the middle line

In order to validate the model, a comparison with the data by Tyagi et al. [30] has been performed and presented in

Figure 5. They studied the same geometry as our work with an inlet velocity of 1 m s^{-1} (MFR=1.198 kg s^{-1}) with a different radiation spectrum, using a nanofluid made of water and alumina nanoparticles, with a volumetric concentration of 0.8% and a particle diameter of 5 nm, and with an initial temperature of 308.15 K.

3. RESULTS AND DISCUSSION

Results in terms of difference of temperature and efficiency of the collector are presented in this chapter.

First, fields of the difference of temperature, in three moments of the day and with two different values of concentration are shown.

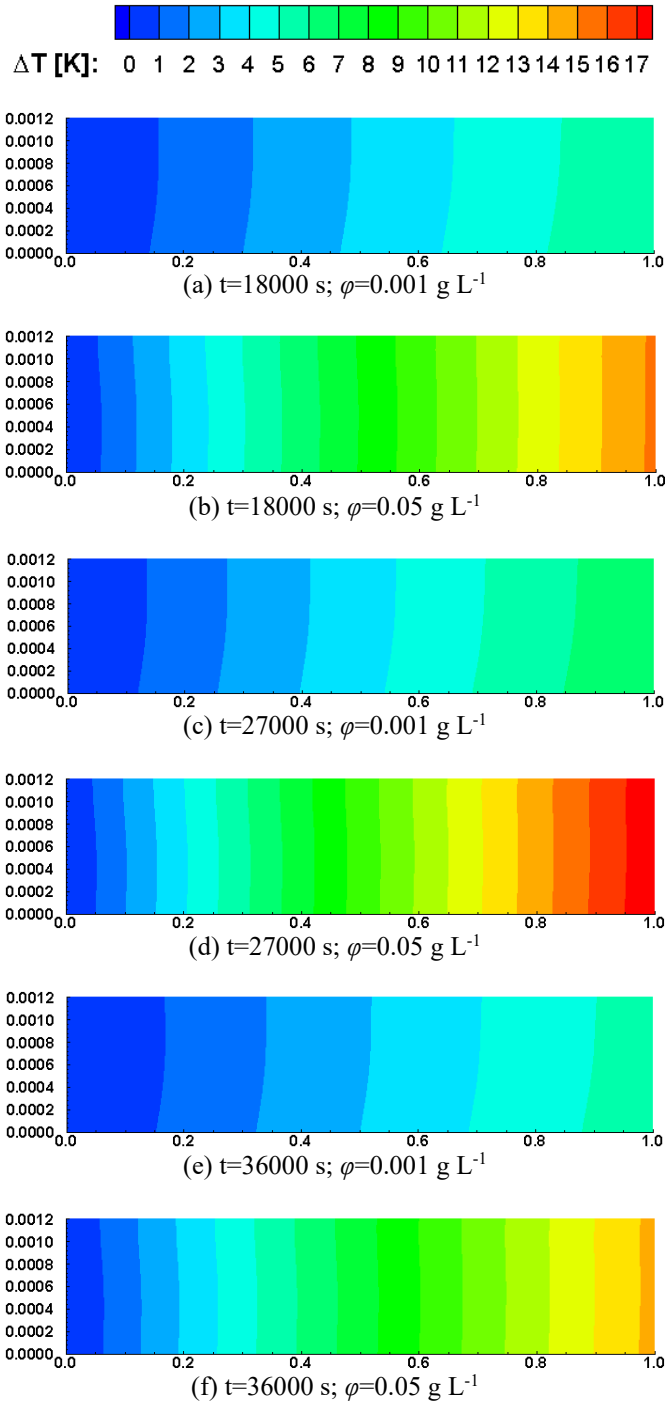

Figure 6. Temperature fields (MFR=0.01 kg s^{-1})

As shown in Figure 6, in all the moments considered, a large difference can be seen between the two different values of concentration considered. Temperature is higher all over the collector with φ=0.05 and its enhancement has a factor of about 3, showing a higher capacity of absorbing for the high concentration nanofluid.

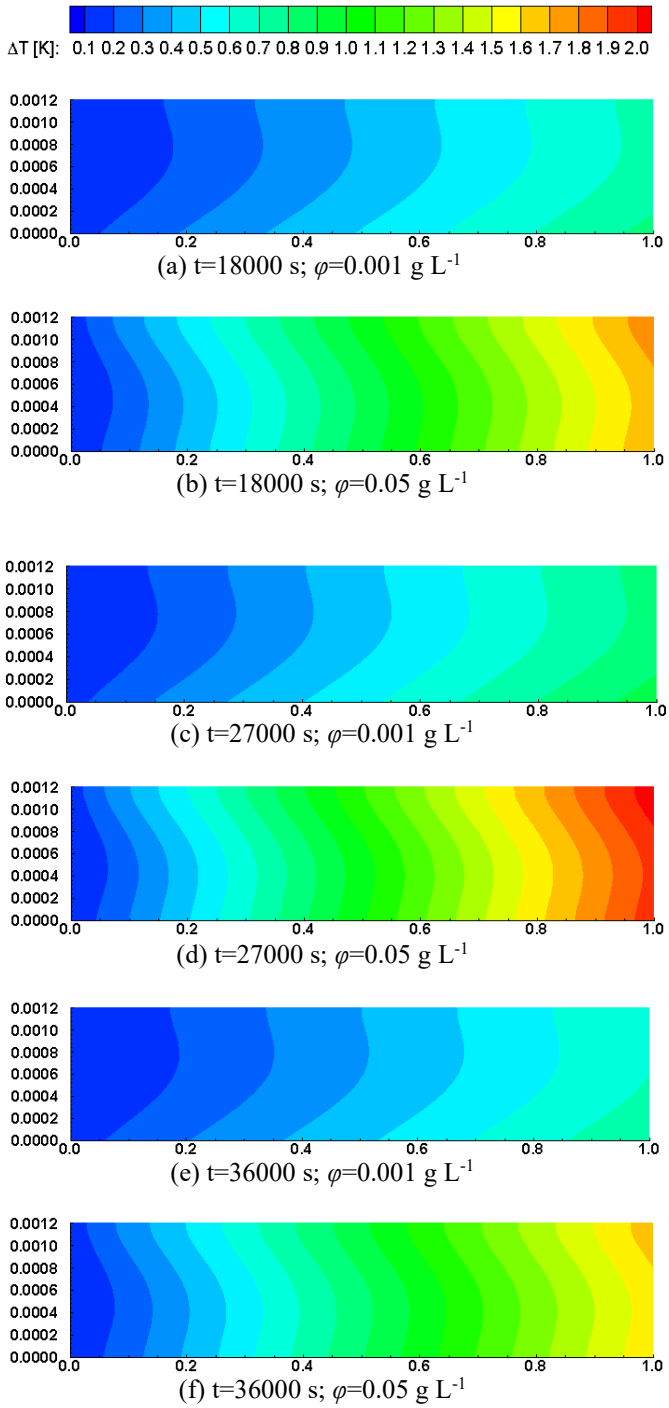

Figure 7. Temperature fields (MFR=0.1 kg s-1)

With MFR=0.1, temperature fields become slightly different, as the temperatures in the cross sections are not uniform. Instead, a minimum on the bottom wall (steel) and a maximum at about y=0.0008 m can be observed with φ=0.001 g L^{-1} (Figures 7a, 7c, and 7e), while with φ=0.05 g L^{-1} (Figures 7b, 7d, and 7f) the trend is inverted, thanks to the high quantity of energy absorbed, with a minimum on the top wall (glass) and a maximum at about y=0.0005 m.

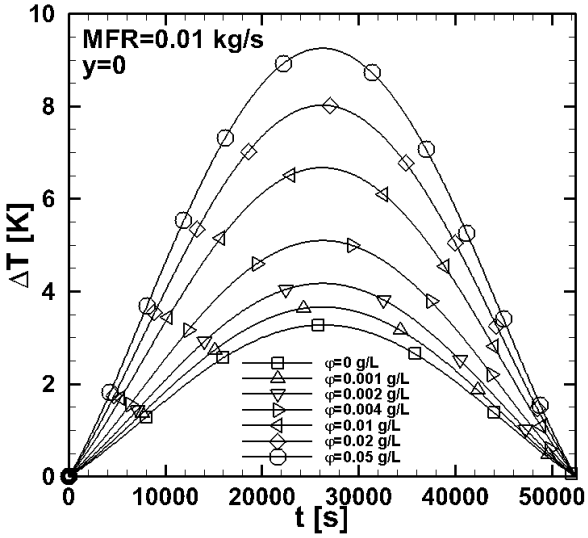

(a) On the bottom wall of the collector

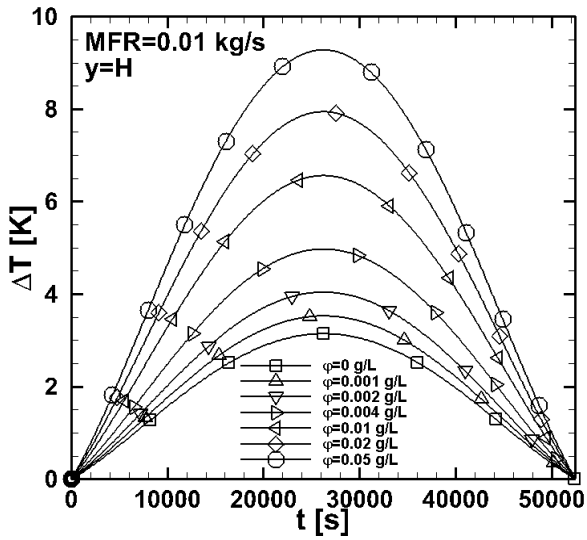

(b) On the top wall of the collector (glass)

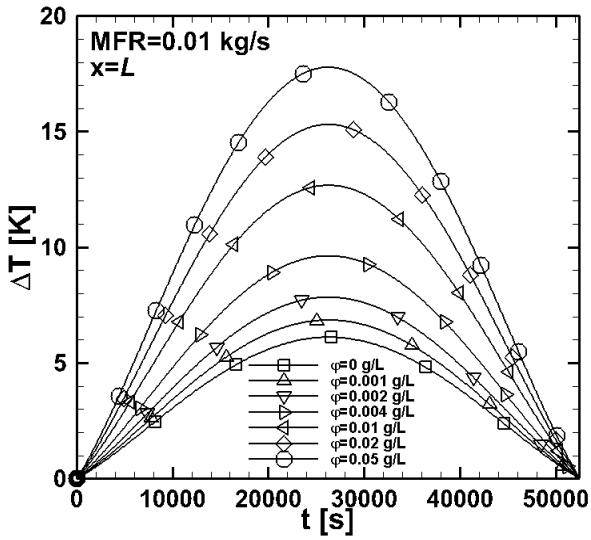

(c) At the exit section

Figure 8. Average temperature against concentration

In Figure 8, the evolution of the average difference temperature on the bottom wall throughout the day is evaluated in three sections of interest (bottom wall, glass and exit section), comparing the results achieved with seven values of concentration of nanoparticles, from 0 (pure water) to 0.05 g L^{-1}. The efficiency of the nanofluid is confirmed by the higher values of ΔT achieved with respect to the water case, with a maximum enhancement of about 300% with φ=0.05 g L^{-1}.

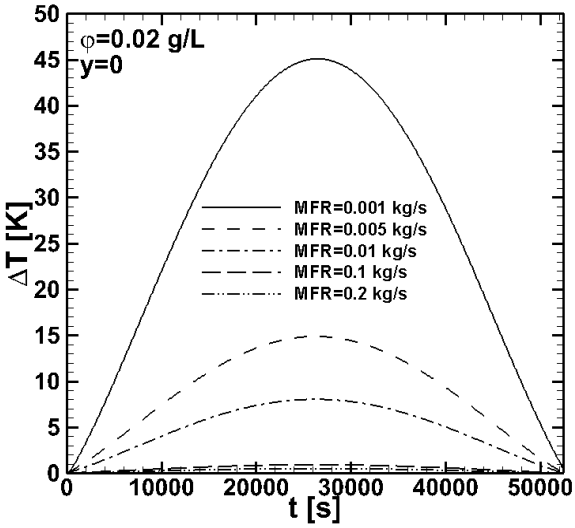

(a) On the bottom wall of the collector

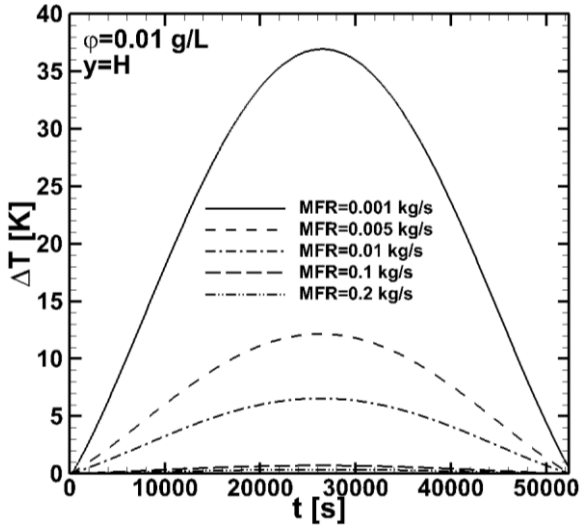

(b) On the top of the collector (glass)

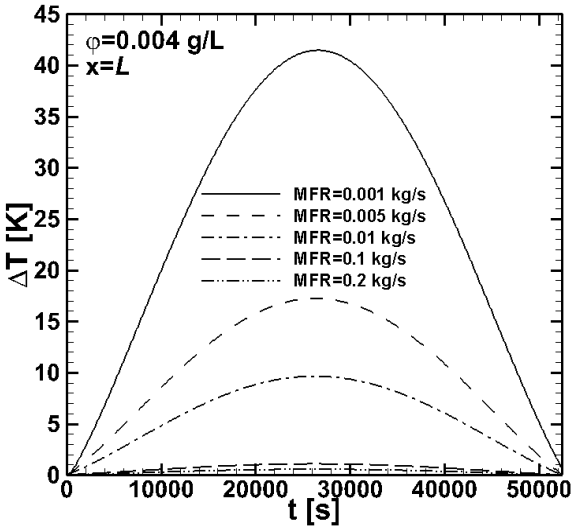

(c) At the exit section

Figure 9. Average temperature against mass flow rate

In Figure 9, average wall temperature has been plotted against the mass flow rate. The inverse proportion between the two parameters can clearly be seen. However, the total energy becomes higher when the MFR is higher: for example, confronting the two lowest values, increasing the MFR by a factor of 5 the ΔT becomes only three times lower.

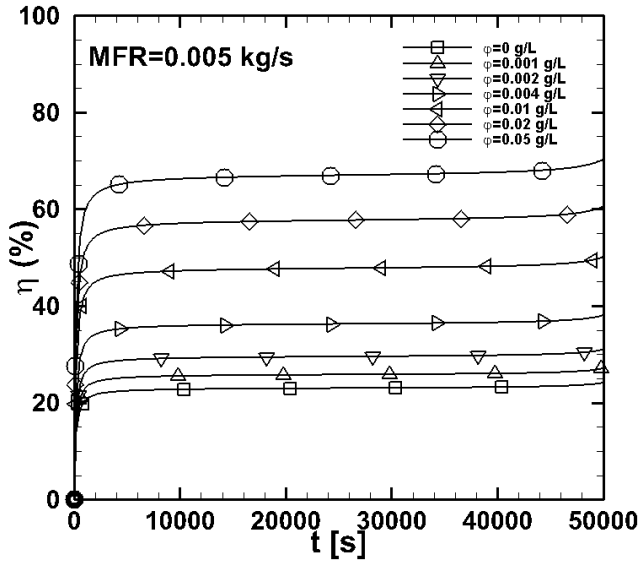

(a) Against concentration

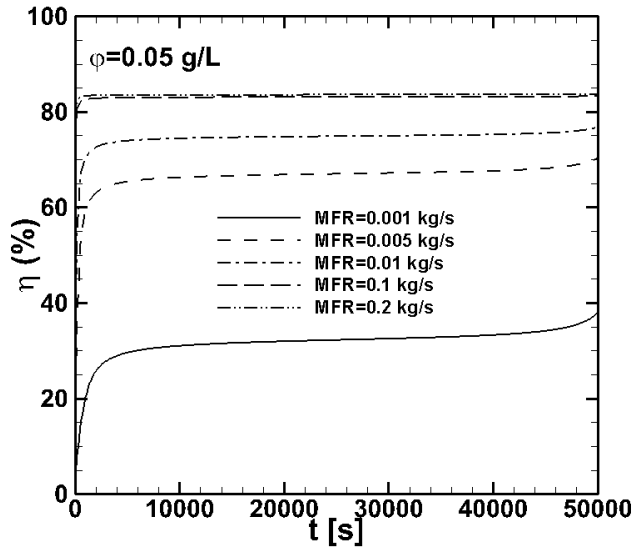

(b) Against mass flow rate

Figure 10. Efficiency of the system

The efficiency of the collector has been calculated following the model of Duffie and Beckman [31]:

$$\eta = \frac{MFR * c_p (T_e - T_i)}{I_T A} \tag{8}$$

where, I_T is the total radiative flux on the top glass and A is the surface area of the glass, while the difference of temperature is calculated using the average temperatures at the exit and the inlet of the collector. This parameter largely increases with the concentration (Figure 10a), reaching values up to 70% at t=50000 s with φ=0.05 g L^{-1}, against the 25% with pure water. The efficiency increases also with the mass flow rate (Figure 10b), reaching an upper limit of about 85% at t=50000 s with MFR=0.2 kg s^{-1}, which is the «maximum of the maximum» obtained in the present work. However, the curves with MFR=0.1 kg s^{-1} and 0.2 kg s^{-1} are very close. As a result, it seems nearly impossible to have a significant improvement over this value.

4. CONCLUSIONS

The results of this study confirm the enhancement of the performance of the DASC when the working fluid is Single-Wall Carbon Nanohorn instead of pure water. This improvement has been demonstrated in terms of temperature difference and thermal efficiency for all values of mass flow rate considered (ranging from 0.001 to 0.02 kg m^{-3}). Additionally, a higher mass flow rate boosts the thermal efficiency of the system, reaching a maximum of approximately 85% for MFR≥0.1 kg s^{-1}. Future developments could involve exploring a collector with a different configuration (such as a varying aspect ratio or a non-zero inclination angle), conducting analyses with radiation in different periods of the year or at various locations on Earth, examining different values of mass flow rate, or even utilizing a different working fluid to explore other concentrations or alternative materials for the base fluid and/or nanoparticles.

ACKNOWLEDGMENT

This work was supported by the Italian Government MUR Grant No. P2022NYPHL – PRIN 2022 PNRR "VISIONS: eVolutIonary deSign of InnOvative heat traNsfer deviceS" – Funded by European Union – Next Generation EU.

REFERENCES

[1] Amar, M., Akram, N., Chaudhary, G.Q., Kazi, S.N., Soudagar, M.E.M., Mubarak, N.M., Kalam, M.A. (2023). Energy, exergy and economic (3E) analysis of flat-plate solar collector using novel environmental friendly nanofluid. Scientific Reports, 13(1): 411. https://doi.org/10.1038/s41598-023-27491-w

[2] Alshuhail, L.A., Shaik, F., Sundar, L.S. (2023). Thermal efficiency enhancement of mono and hybrid nanofluids in solar thermal applications–A review. Alexandria Engineering Journal, 68: 365-404. https://doi.org/10.1016/j.aej.2023.01.043

[3] Masuda, H., Ebata, A., Teramae, K. (1993). Alteration of thermal conductivity and viscosity of liquid by dispersing ultra-fine particles. Dispersion of Al_2O_3, SiO_2 and TiO_2 ultra-fine particles. Netsu Bussei, 7(4): 227-233. https://sid.ir/paper/596250/en.

[4] Choi, S.U., Eastman, J.A. (1995). Enhancing thermal conductivity of fluids with nanoparticles. In 1995 International mechanical engineering congress and exhibition, San Francisco, United States, No. ANL/MSD/CP-84938; CONF-951135-29.

[5] Otanicar, T.P., Phelan, P.E., Golden, J.S. (2009). Optical properties of liquids for direct absorption solar thermal energy systems. Solar Energy, 83(7): 969-977. https://doi.org/10.1016/j.solener.2008.12.009

[6] Burgos, J., Mondragón, R., Elcioglu, E.B., Fabregat-Santiago, F., Hernández, L. (2022). Experimental

characterization and statistical analysis of water-based gold nanofluids for solar applications: Optical properties and photothermal conversion efficiency. Solar RRL, 6(7): 2200104. https://doi.org/10.1002/solr.202200104

[7] Mondragón, R., Burgos, J., Hernández, L., Manca, O., Sarli, G., Palma, R. (2023). Finite element formulation applied to solar nanofluid for direct absorption solar collectors. In 13th National and 4th International Conference in Engineering Thermodynamics, Castellón de la Plana, Spain.

[8] Burgos, J., Mondragón, R., Martínez-Cuenca, R., Nithiyanantham, U., Barison, S., Mancin, S., Fabregat-Santiago, F., Hernández, L. (2023). Photothermal properties and performance of hybrid carbon-paraffin/water emulsions. Journal of Energy Storage, 73: 109136. https://doi.org/10.1016/j.est.2023.109136

[9] Kumar, K.P., Khedkar, R., Sharma, P., Elavarasan, R.M., Paramasivam, P., Wanatasanappan, V.V., Dhanasekaran, S. (2024). Artificial intelligence-assisted characterization and optimization of red mud-based nanofluids for high-efficiency direct solar thermal absorption. Case Studies in Thermal Engineering, 54: 104087. https://doi.org/10.1016/j.csite.2024.104087

[10] Sani, E., Dell'Oro, A. (2014). Optical constants of ethylene glycol over an extremely wide spectral range. Optical Materials, 37: 36-41. https://doi.org/10.1016/j.optmat.2014.04.035

[11] Çobanoğlu, N., Karadeniz, Z.H., Turgut, A. (2019). Carbon-based nanofluid applications in solar thermal energy. In E3S Web of Conferences (CLIMA 2019), Bucharest, Romania, 111: 01056. https://doi.org/10.1051/e3sconf/201911101056

[12] Yu, L.F., Shang, Z.C., Lin, X.C., Li, M.X, Liu, Y.B., Ren, L.T., Deng, S.S., Zhang, F., Luo, L., Duan, H.H., Sun, X.M. (2023). Bio-Derived wood-based gas diffusion electrode for high-performance aluminum–Air batteries: Insights into pore structure. Advanced Materials Interfaces, 11(1): 2300355. https://doi.org/10.1002/admi.202300355

[13] Zanetti, E., Dugaria, S., Biscaglia, F., Agresti, F., Fedele, L., Meneghetti, M., Del Col, D. (2021). Investigation of nanofluids circulating in a volumetric solar receiver. Journal of Thermal Science and Engineering Applications, 13(4): 041023. https://doi.org/10.1115/1.4049041

[14] Berto, A., Zanetti, E., Ponzana, G., Meneghetti, M., Del Col, D. (2022). In-line measurement of absorbed solar irradiance using a volumetric collector with SWCNH nanofluid. Heat and Mass Transfer, 1-13. https://doi.org/10.1007/s00231-022-03271-6

[15] Askari, S., Lotfi, R., Seifkordi, A., Rashidi, A.M., Koolivand, H. (2016). A novel approach for energy and water conservation in wet cooling towers by using MWNTs and nanoporous graphene nanofluids. Energy Conversion and Management, 109: 10-18. https://doi.org/10.1016/j.enconman.2015.11.053

[16] Sharaf, O.Z., Kyritsis, D.C., Abu-Nada, E. (2018). Impact of nanofluids, radiation spectrum, and hydrodynamics on the performance of direct absorption solar collectors. Energy Conversion and Management, 156: 706-722. https://doi.org/10.1016/j.enconman.2017.11.056

[17] Abu-Zeid, M.A.R., Elhenawy, Y., Bassyouni, M., Majozi, T., Toderas, M., Al-Qabandi, O.A., Kishk, S.S. (2024). Performance enhancement of flat-plate and parabolic trough solar collector using nanofluid for water heating application. Results in Engineering, 21: 101673. https://doi.org/10.1016/j.rineng.2023.101673

[18] Sreekumar, S., Shaji, J., Cherian, G., Thomas, S., Mondol, J.D., Shah, N. (2024). Corrosion analysis and performance investigation of hybrid MXene/C-dot Nanofluid-Based direct absorption solar collector. Solar Energy, 269: 112317. https://doi.org/10.1016/j.solener.2024.112317

[19] Sattar, A., Bofeng, B., Fazal, F., Farooq, M., Riaz, F., Hussain, I., Khan, M.I. (2024). Experimental investigation of photothermal performance in nanofluid-based direct absorption solar collection for solar-driven water desalination. Case Studies in Thermal Engineering, 59: 104464. https://doi.org/10.1016/j.csite.2024.104464

[20] Gupta, V.K., Kumar, S., Kukreja, R., Chander, N., Ravi, R.K. (2024). Real-time thermal performance investigation of a thermal energy storage integrated direct absorption solar collector under tropical climate. Energy Storage, 6(1): e567. https://doi.org/10.1002/est2.567

[21] Shahini, N., Karami, M., Akhavan-Behabadi, M.A. (2024). CFD modeling of a triple-walled direct absorption evacuated tube solar collector based on hybrid nanofluid/microencapsulated PCM. Energy Science & Engineering, 12(5): 2297-2318. https://doi.org/10.1002/ese3.1741.

[22] Simonetti, M., Restagno, F., Sani, E., Noussan, M. (2020). Numerical investigation of direct absorption solar collectors (DASC), based on carbon-nanohorn nanofluids, for low temperature applications. Solar Energy, 195: 166-175. https://doi.org/10.1016/j.solener.2019.11.044

[23] Hasan, A., Alazzam, A., Abu-Nada, E. (2024). Direct absorption solar collectors: Fundamentals, modeling approaches, design and operating parameters, advances, knowledge gaps, and future prospects. Progress in Energy and Combustion Science, 103: 101160. https://doi.org/10.1016/j.pecs.2024.101160

[24] Sani, E., Barison, S., Pagura, C., Mercatelli, L., Sansoni, P., Fontani, D., Jafrancesco, D., Francini, F. (2010). Carbon nanohorns-based nanofluids as direct sunlight absorbers. Optics Express, 18(5): 5179-5187. https://doi.org/10.1364/OE.18.005179

[25] Taylor, R.A., Phelan, P.E., Otanicar, T.P., Adrian, R., Prasher, R. (2011). Nanofluid optical property characterization: Towards efficient direct absorption solar collectors. Nanoscale Research Letters, 6: 1-11. https://doi.org/10.1186/1556-276X-6-225

[26] Hale, G.M., Querry, M.R. (1973). Optical constants of water in the 200-nm to 200-μm wavelength region. Applied Optics, 12(3): 555-563. https://doi.org/10.1364/AO.12.000555

[27] Solar spectrum calculator. https://www2.pvlighthouse.com.au/calculators/solar%20spectrum%20calculator/solar%20spectrum%20calculator.aspx, accessed on Apr. 23, 2024.

[28] ANSYS Fluent Tutorial Guide (2020 R2 Release). http://www.ansys.com.

[29] Patankar, S.V. (1980). Numerical heat transfer and fluid flow. New York, NY, USA: Hemisphere Publishing Corporation. https://doi.org/10.1201/9781482234213

[30] Tyagi, H., Phelan, P., Prasher, R. (2009). Predicted

efficiency of a low-temperature nanofluid-based direct absorption solar collector. Journal of Solar Energy Engineering, 131(4): 041004. https://doi.org/10.1115/1.3197562
[31] Duffie, J.A., Beckman, W.A. (2013). Solar Engineering of Thermal Processes. John Wiley & Sons. https://doi.org/10.1002/9781118671603

NOMENCLATURE

A	surface area, m^2
cp	specific heat, J. kg^{-1} K^{-1}
d	density, kg m^{-3}
DO	Discrete Ordinates
f	function
H	height of the collector, m
I	intensity of light, W m^{-2}
L	length of the collector, m
k	thermal conductivity, W m^{-1}. K^{-1}
K	extinction coefficient, m^{-1}
MFR	mass flow rate, kg s^{-1}
n	refractive index
p	pressure, Pa
RTE	radiative transfer equation
t	time, s
T	temperature, K
Q_R	radiative heat flux, W m^{-2}
u, v	x and y velocity components, m s^{-1}
x, y	Cartesian coordinates, m

Greek symbols

φ	concentration of the nanoparticles, g L^{-1}
λ	wavelength, nm
μ	dynamic viscosity, kg m^{-1} s^{-1}
ν	kinematic viscosity
ρ	reflectance
τ	transmittance

Subscripts

0	initial
b	bottom plate
e	exit
g	glass
i	inlet
t	total
nf	nanofluid